7

Parton theory: further developments

In the previous chapter, we formalized the parton model in a simple quantum field theory. A number of further developments follow fairly simply, and this chapter's purpose is to give an account of them, before we go on to the full QCD treatment.

We first extend the parton model for DIS to the very important case of charged-current weak-interaction processes. Then we examine a particularly influential form of perturbation theory: light-front (or x^+-ordered) perturbation theory. After that I present the light-front quantization of gauge theories, a natural extension of what we did earlier for non-gauge theories. We will thereby be able to introduce appropriate definitions for parton densities in a gauge theory, and to convert them to a gauge invariant form with the aid of what are known as Wilson-line operators.

7.1 DIS with weak interactions, neutrino scattering, etc.

We have extensively discussed DIS for the case of virtual photon exchange. The same principles apply equally to all lepto-production processes $l + N \longrightarrow l' + X$, and thus they apply whether the exchanged electroweak boson is a W, Z or photon. There are a large number of different cases, and, as far as the theory by itself is concerned, all are a minor variation on the purely electromagnetic case, both at the parton-model level, and with all the QCD modifications. The structure-function review in Amsler *et al.* (2008, Ch. 16) is an authoritative source for the relevant results including corrections of errors in the literature and commonly used standards for notations, the bulk of which we follow. See also Hobbs and Melnitchouk (2008) for a recent treatment of the role of γ–Z interference in the parity-violating part of neutral current DIS.

7.1.1 Structure functions

In view of its particular importance to the determination of the flavor-separated quark densities, we restrict our attention to the charged-current processes in neutrino scattering on unpolarized nucleons. These are the processes $\nu + N \longrightarrow \mu + X$ and $\nu + N \longrightarrow e + X$, with the exchanged boson being the W^+. The hadronic tensor is

$$W^{\mu\nu}(q, P) = \frac{1}{4\pi} \int d^4z \ e^{iq \cdot z} \langle P, S| J^\mu(z/2)^\dagger J^\nu(-z/2) |P, S\rangle, \qquad (7.1)$$

213

where J is now the non-hermitian hadronic current coupling to the W boson. We normalize this charge-changing current to

$$J^\mu = \bar{u}\gamma^\mu(1 - \gamma_5)d' + \bar{c}\gamma^\mu(1 - \gamma_5)s' + \bar{t}\gamma^\mu(1 - \gamma_5)b'$$

$$= \begin{pmatrix} \bar{u} & \bar{c} & \bar{t} \end{pmatrix} \gamma^\mu(1 - \gamma_5) U_{\text{CKM}} \begin{pmatrix} d \\ s \\ b \end{pmatrix}. \tag{7.2}$$

Here u, c, and t are the fields for the corresponding quarks, and d', s', and b' are for the down-type quarks that are associated with them in multiplets of weak isospin. The fields for *mass-eigenstate* quarks, d, etc., are obtained by a CKM rotation, reviewed in Amsler *et al.* (2008, Ch. 11), and implemented in the above equation by the matrix U_{CKM}, which acts on quark flavor indices.

We next decompose $W^{\mu\nu}$ in scalar structure functions. There are two differences compared with the pure electromagnetic case, both of which increase the number of structure functions. First is that parity is not conserved and second is that the currents are not conserved because the quark masses are non-zero. A thorough analysis was given by Ji (1993), who found 14 structure functions on a spin-$\frac{1}{2}$ hadron target, of which 5 appear when the hadron is unpolarized and 9 concern hadron-polarization dependence.

For most purposes we can neglect the structure functions allowed by non-conservation of the current. Normally, we neglect quark masses compared with Q within the hard scattering, so that the extra structure functions are suppressed by a power of m_q/Q. This of course does not always work for heavy quarks, notably the b and t.

Thus the extra structure functions could be significant when there is a heavy quark in the hard scattering. However, the associated tensors almost all have a factor of q^μ or q^ν, the one exception being in polarized scattering. Now a factor q^μ or q^ν times the leptonic tensor is non-zero only because a lepton mass is non-zero, and therefore we obtain a suppression by a power of a small *lepton* mass divided by Q.

The result is that for neutrino scattering on an unpolarized target, we have one extra relevant structure function F_3:

$$W^{\mu\nu} = \left(-g^{\mu\nu} + q^\mu q^\nu/q^2\right) F_1(x, Q^2) + \frac{(P^\mu - q^\mu P \cdot q/q^2)(P^\nu - q^\nu P \cdot q/q^2)}{P \cdot q} F_2(x, Q^2)$$

$$- i\epsilon^{\mu\nu\alpha\beta} \frac{q_\alpha P_\beta}{2 P \cdot q} F_3(x, Q^2) + \text{irrelevant}. \tag{7.3}$$

See Amsler *et al.* (2008, Ch. 16) for a definition that includes structure functions for polarized scattering.

7.1.2 Parton model with low-mass quarks

The parton model and its derivation work equally well with neutrino scattering at large Q. As before, the parton-model approximation to the hadronic tensor is just a sum over parton densities times the tensor computed to lowest order on an on-shell quark target, as
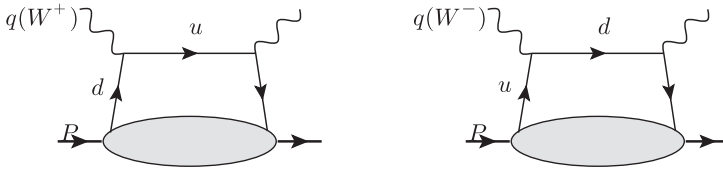
Fig. 7.1. Examples of lowest-order parton-model processes for charged-current DIS with a W^+ or a W^- exchanged.

in (2.27). Let $\hat{k}^\mu = (x P^+, 0, \mathbf{0}_T)$ be the approximated quark momentum. Then the partonic tensor (2.28) is simply replaced by

$$C_j^{\mu\nu} = \frac{1}{4\pi} \frac{1}{2} \operatorname{Tr} \hat{k} \gamma^\mu (1 - \gamma_5)(\slashed{q} + \hat{k})\gamma^\nu(1 - \gamma_5)\, 2\pi \delta((q + \hat{k})^2), \qquad (7.4)$$

with the restriction to the allowed partonic subprocesses, e.g., $d \to u$, $\bar{u} \to \bar{d}$, etc. for W^+ exchange. Note that the formula must be slightly changed on an antiquark. It is readily deduced that the parton-model structure functions are

$$F_2^{\mathrm{QPM}, W^+} = 2x\, [d(x) + \bar{u}(x) + s(x) + \bar{c}(x) + \ldots], \qquad (7.5a)$$

$$F_1^{\mathrm{QPM}, W^+} = \frac{1}{2x} F_2, \qquad (7.5b)$$

$$F_3^{\mathrm{QPM}, W^+} = 2\, [d(x) - \bar{u}(x) + s(x) - \bar{c}(x) + \ldots]. \qquad (7.5c)$$

For processes like $\bar{\nu} p \to e^+ X$ with W^- exchange, the roles of the quarks in each isospin doublet are exchanged, to give

$$F_2^{\mathrm{QPM}, W^-} = 2x\, \left[u(x) + \bar{d}(x) + \bar{s}(x) + c(x) + \ldots\right], \qquad (7.6a)$$

$$F_1^{\mathrm{QPM}, W^-} = \frac{1}{2x} F_2, \qquad (7.6b)$$

$$F_3^{\mathrm{QPM}, W^-} = 2\, \left[u(x) - \bar{d}(x) - \bar{s}(x) + c(x) + \ldots\right]. \qquad (7.6c)$$

Only those heavy quarks whose mass is low enough to participate in the process should be included. Notice the restricted set of quark flavors allowed in each structure function (Fig. 7.1). Notice also the reversal of sign for the antiquark terms in the F_3 structure function. These properties indicate how important charged-current scattering is for the flavor separation of quark and antiquark densities from data.

7.1.3 Quark masses

So far our arguments have relied on Q being much larger than all the particle masses of a theory; the reduced diagram analysis concerned the zero-mass limit $m/Q \to 0$. But the wide range of quark masses in QCD shows that there is an interesting region where Q is much larger than the lightest masses, but less than or comparable to some of the heavy quark masses. A full and systematic treatment in QCD will appear in Sec. 11.7.

Charged-current DIS, where heavy quarks can be produced off light quarks, provides a useful place to initiate the discussion of heavy quarks. The basic methodology is to treat the heavy quark masses as a large scale, just like Q. Then we apply the Landau analysis to locate the PSSs only for the light partons. The heavy quarks appear only inside the hard scattering, and the parton densities used are for light partons only. Naturally, when Q is increased sufficiently above the mass of a particular quark, the status of the quark changes.

For neutral-current processes, heavy quarks are made in pairs, and the hard scattering analysis is closely tied to the higher-order corrections to the hard scattering, to be studied later. But for charged-current processes, the production of a heavy quark can occur at lowest order, e.g., $W^- + \bar{s} \to \bar{c}$, $W^+ + s \to c$. Then the parton-model approximation for the hard scattering retains the massless approximation for the incoming quark, but we insert the mass m_h for the outgoing heavy quark. Thus we replace the parton-level structure function (7.4) by

$$C_j^{\mu\nu} = \frac{1}{4\pi} \frac{1}{2} \operatorname{Tr} \hat{k} \gamma^\mu (1 - \gamma_5)(\slashed{q} + \hat{\slashed{k}} + m_h) \gamma^\nu (1 - \gamma_5) \, 2\pi \delta((q + \hat{k})^2 - m_h^2), \qquad (7.7)$$

applicable to a process $W + q_j \to q_h$, with a transition from a light quark of flavor j to a heavy quark h. The mass shell condition now sets the parton momentum fraction to

$$\xi = x(1 + m_h^2/Q^2) \qquad (7.8)$$

rather than simply x. It can readily be checked that the contributions to the hadronic structure functions are

$$F_1^{j\to h} = f_j(\xi), \qquad F_2^{j\to h} = 2\xi f_j(\xi), \qquad F_3^{j\to h} = 2 f_j(\xi). \qquad (7.9)$$

This should be used to replace the relevant terms in (7.5) and (7.6).

In addition there are terms in (7.7) proportional to $q^\mu q^\nu/Q^2$ and $(P^\mu q^\nu + q^\mu P^\nu)/P \cdot q$, which are allowed because of non-conservation of the currents when quark masses are non-zero. As already stated, the factors of q^μ or q^ν multiply the leptonic tensor, and give a suppression by a power of *lepton* mass divided by Q.

There is in principle a sharp structure in the structure functions at the threshold for production of a heavy quark, at

$$x_{\text{exact threshold}} = \frac{1}{1 + (M_{\text{min}}^2 - M^2)/Q^2}, \qquad (7.10)$$

where M_{min} is the lowest-mass final state in $W^\pm + P \to X$ that includes a hadron containing a particular heavy quark. For a b quark this might be the lightest B-flavored baryon, Λ_b^0. In contrast the partonic calculation gives a threshold in x given by setting $\xi = 1$ in (7.8), i.e., at

$$x_{\text{parton threshold}} = \frac{1}{1 + m_h^2/Q^2}. \qquad (7.11)$$

This differs from the exact threshold because the heavy baryon's mass is not exactly equal to the heavy quark's mass and because there is an effect due to the proton mass,

both effects being neglected in the partonic calculation. For practical purposes the difference is not important because the parton densities vanish strongly at $\xi = 1$ and the main contributions arise from small ξ. Thus the main numerical contributions to the structure functions from heavy quark occur for values of x well beyond the threshold for heavy quark production.

Even so, the disagreement between the thresholds in x illustrates a principle mentioned in our derivation of the parton model in Sec. 6.1.1. This is that the approximations only apply to a local average of the structure functions, which would smear out sharp structures. Observe that the exact and parton-model thresholds in x differ by an amount proportional to hadronic-mass-squared divided by Q^2, a power-suppressed quantity. This is an important principle to remember whenever thresholds appear in partonic calculations. Improvements can only be made by treating parton kinematics better.

7.2 Light-front perturbation theory

In analyzing a collinear region, a number of interesting simplifications arise when we integrate over the minus components of loop momenta. A simple example was in Sec. 6.11.5 for a one-loop calculation of a parton density, where it gave the restriction that fractional momenta for internal lines correspond to forward-moving particles: the target splits into two forward-moving partons, both with positive plus momentum, and one of the partons initiates the hard scattering.

In the example, and as we will now see quite generally for any Feynman graph, integrating over the minus momenta led to restrictions on plus momenta that correspond to to the restrictions imposed by the reduced graph analysis of Ch. 5. This leads to an interesting generalization of the method of time-ordered perturbation theory (Sterman, 1993, Sec. 9.5). In this older method, in contrast to Feynman perturbation theory, the effect of interactions is to cause transitions from one state to another, the interactions occur as a sequence in time, and there are energy denominators corresponding to the intermediate states. Time-ordered perturbation theory gives a useful intuition as to the time evolution of the system's state. But in relativistic theories time-ordered perturbation theory is inefficient (Heinzl, 2007), because a Feynman graph with n vertices has $n!$ time orderings. If time ordering is replaced by ordering in x^+, it turns out that many of the orderings of the vertices give zero. This formulation corresponds to a natural version of perturbation theory within light-front quantization, when the role of time in ordinary quantum-mechanical evolution equations is replaced by evolution in x^+.

The method arose first – see Brodsky, Pauli, and Pinsky (1998) for a review – in the use of what was called the "infinite-momentum" frame for understanding the parton model. The systematization in terms of light-front variables and then x^+-ordered perturbation theory was made by Chang and Ma (1969) and Kogut and Soper (1970). Chang and Ma also showed how the rules arise by performing the k^- integrals in Feynman graphs.

Naturally, if one wishes to discuss collinear regions with the high-energy particle(s) moving in some direction other than the $+z$ direction, a different definition of light-front coordinates is appropriate.
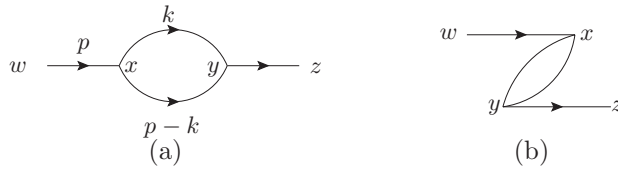
Fig. 7.2. (a) Self-energy graph. (b) An x^+ ordering that gives zero.

7.2.1 Example

The basic principles are illustrated by the simple example of the propagator correction graph in ϕ^3 theory, shown in Fig. 7.2(a). We first examine the case that the external momentum obeys $p^+ > 0$. Since we need to consider also the graphs in coordinate space, each vertex is labeled with a position variable. The value of the graph is

$$\Gamma(p) = \frac{-g^2}{(p^2 - m^2)^2 \, 2(2\pi)^n} \int \mathrm{d}^n k \, \frac{1}{2k^+ k^- - k_{\mathrm{T}}^2 - m^2 + i0}$$
$$\times \frac{1}{2(p^+ - k^+)(p^- - k^-) - (\boldsymbol{p}_{\mathrm{T}} - \boldsymbol{k}_{\mathrm{T}})^2 - m^2 + i0}. \tag{7.12}$$

We perform the integral over k^- by closing the contour in the upper or lower half plane. This gives zero except when k^+ is between 0 and p^+, with the result

$$\Gamma(p) = \frac{(-ig)^2}{2(2\pi)^{n-1}} \int_0^{p^+} \mathrm{d}k^+ \int \mathrm{d}^{n-2} \boldsymbol{k}_{\mathrm{T}} \, \frac{1}{(2p^+)^2 \, 2k^+ \, 2(p^+ - k^+)}$$
$$\times \frac{i^3}{\left[p^- - \dfrac{\boldsymbol{p}_{\mathrm{T}}^2 + m^2}{2p^+} + i0 \right]^2 \left[p^- - \dfrac{\boldsymbol{k}_{\mathrm{T}}^2 + m^2}{2k^+} - \dfrac{(\boldsymbol{p}_{\mathrm{T}} - \boldsymbol{k}_{\mathrm{T}})^2 + m^2}{2(p^+ - k^+)} + i0 \right]}. \tag{7.13}$$

This has been organized so as to correspond to the general form we will find in x^+-ordered perturbation theory. The relevant ordering is given in Fig. 7.2(a). This has three intermediate states, between the vertices w and x, between x and y, and between y and z. The last line of (7.13) is a product of an energy denominator factor for each intermediate state. Each of these factors is $i/(p^- - \text{on-shell} + i0)$, where "on-shell" denotes the value of minus momentum the state would have if the particles were on-shell. Note that two of the denominators, for the first and last intermediate states, are equal. In common with the Feynman-graph method, there are the factors of $-ig$ for each vertex and a symmetry factor $\frac{1}{2}$. The integration is only over the plus and transverse momenta, and for each line there is a factor of one divided by twice its plus momentum. This corresponds to the denominator in the light-front version of the "Lorentz-invariant phase-space" measure, (6.59). At each internal vertex are conserved the independent components of momentum needed to specify physical states, i.e., the plus and transverse components.

In advance of their general proof, we can use this graph as an illustration of the results that yield the main simplifications given by light-front perturbation theory. Each line has to carry a physical positive value of plus momentum, when considered flowing from left to right. Because $p^+ > 0$, the x vertex is to the right of the w vertex, and similarly for z relative to y, i.e., $x^+ > w^+$, $z^+ > y^+$. This still leaves one other possible ordering, shown in Fig. 7.2(b), where y^+ is earlier than x^+. However, this ordering does not give an allowed situation, since at the x vertex we have three positive plus momenta coming in from the left and none going out to the right. This is how the simplification compared with time-ordered perturbation theory occurs. With time-ordered perturbation theory, the ordinary energy k^0 would have been integrated over, and the independent variables for each line would be the ordinary spatial momentum, none of whose components has any constraint on its sign.

For this one Feynman graph we have one x^+ ordering that gives a non-zero result. In contrast, time-ordered perturbation theory would have $4! = 24$ time orderings for the same Feynman graph.

One can readily verify that the above calculation reproduces the standard result for the Feynman graph by performing the $\boldsymbol{k}_T$ integral. After a change of variable to $x = k^+/p^+$, an integral is obtained that is the same as is obtained when the momentum integral in (7.12) is performed by the conventional Feynman parameter method.

7.2.2 Paradox at $p^+ = 0$

We obtained (7.13) for the case that p^+ was positive, and observed that it gives the correct value. Similarly when p^+ is negative, we also get the correct value, but with a reversed ordering for the vertices.

But if p^+ is exactly zero, the poles in k^- in the original integral (7.12) are either both in the lower half plane (if $k^+ > 0$) or both in the upper half plane (if $k^+ < 0$). Completing the contour of k^- away from the poles then gives zero for all values of k^+. This disagrees with the definite non-zero limit of (7.13) as $p^+ \to 0$, and hence with the non-zero value of the ordinary Feynman graph.

This issue is rather important, because the same method can be used to show that disconnected vacuum bubbles are apparently all zero in light-front perturbation theory e.g., Weinberg (1966) and the *introduction* (but not the later sections) of Chang and Ma (1969). This has contributed to a general impression (e.g., Brodsky, Pauli, and Pinsky, 1998) that the vacuum is trivial in light-front quantization, unlike the case for equal-time quantization; i.e., the interactions do not change the vacuum state. Now, although vacuum bubbles are normally discarded, they physically give an energy density to the vacuum, which can be related to the energy-momentum tensor in the vacuum. Vacuum energy-momentum is equivalent (Weinberg, 1989) to a contribution to the cosmological constant in general relativity, i.e., it has observable consequences. (There is, of course, an infinite renormalization of the cosmological constant to cancel UV divergences in vacuum bubbles.) Evidently, when different results are obtained for the same graph by different methods of calculation in the same theory, at least one method is wrong.
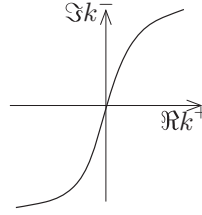
Fig. 7.3. Partially deformed contour for evaluation of integral at zero external p^+. Note that the axes are the real part of k^+ and the imaginary part of the *other* variable k^-, and that there are therefore two other dimensions not shown, for $\Re k^-$ and $\Im k^+$.

Our propagator calculation indicates that there must be a problem with the derivation of a zero value for the propagator correction at zero external plus momentum, since that disagrees with the limit from non-zero p^+, and propagators are analytic functions of external momentum. This problem was recognized and solved, at least in examples, by Chang and Ma (1969). A more general solution was provided by Yan (1973) with generalizations by Heinzl (2003).

At zero external p^+ we need the integral over k^- and k^+ of

$$\frac{1}{[2k^+k^- - k_{\mathrm{T}}^2 - m^2 + i0]\,[2k^+(k^- - p^-) - (\boldsymbol{p}_{\mathrm{T}} - \boldsymbol{k}_{\mathrm{T}})^2 - m^2 + i0]}. \tag{7.14}$$

We deform the (*two-real-dimensional*) contour of integration so that the imaginary part of k^- is infinite and positive when $k^+ > 0$, but infinite and negative when $k^+ < 0$. As illustrated in Fig. 7.3, the contour of integration is a connected manifold and so at k^+ close to zero, the deformed contour has to pass through small values of $\Im k^-$. This leaves the possibility of a non-zero contribution, where k^+ is very small and k^- is very large, leaving k^+k^- of a fixed size. (Such a contribution does not arise when the external plus momentum is non-zero, because there is then a large denominator containing a p^+k^- term.)

Contour integration shows that the integral over k^- of (7.14) is zero whenever k^+ is non-zero. On the other hand the integral of (7.14) over both k^+ and k^- is definitely non-zero. This indicates that the integral over the one variable k^- must be treated as a generalized function of the other variable k^+, e.g., a coefficient times $\delta(k^+)$: it is zero everywhere except at one point, but with a non-zero integral. In fact, Yan (1973) and Heinzl (2003) showed that

$$\int \mathrm{d}k^- \frac{1}{(M^2 - 2k^+k^- - i0)^\nu} = \pi i \frac{\delta(k^+)}{(\nu - 1)(M^2)^{\nu-1}}. \tag{7.15}$$

This formula can be used to calculate the integral of (7.14) with the aid of a Feynman parameter combination for the denominators, and results in agreement with the Feynman-graph calculation and with the limit from $p^+ \neq 0$. The paradox is now resolved.

For disconnected vacuum diagrams, this solves the disagreement between light-front perturbation theory and regular Feynman perturbation theory; Feynman perturbation theory is correct, and there is in this case little notable advantage to use of light-front perturbation theory.

But for graphs with non-zero external momenta, we can choose the external momenta to avoid the problematic situations, as was shown quite generally by Chang and Ma (1969). We avoid the problems if no subgraph is forced by the configuration of external momenta to have exactly zero for its external plus momentum.

Certain other complications arise when there are numerator factors with dependence on k^-. These can affect the convergence of the k^- integrals, and a naive application of light-front methods to a Feynman graph can give a wrong result. This is particularly the case for calculations in a massless on-shell approximation.

7.2.3 General rules

Statement

The general rules for perturbation theory in the x^+-ordered form can be found in Chang and Ma (1969), Kogut and Soper (1970), and Yan (1973), but with a different normalization. There are some complications associated with momentum dependence in vertices and in propagator numerators, so we first state and derive the rules for scalar theories.

1. The graphs are like Feynman graphs except that the vertices are assigned an ordering in x^+, which in drawing diagrams we will take to increase from left to right. All possible graphs and orderings are to be used.
2. Coupling factors at vertices and symmetry factors are the same as in Feynman graphs.
3. Each line l is assigned a plus and transverse momentum: k_l^+, $\boldsymbol{k}_{l\mathrm{T}}$, and these components of momentum are subject to conservation at the vertices.
4. The sign of each line momentum is chosen to correspond to propagation from lower to higher x^+, and then k_l^+ is always physical, i.e., positive.
5. For each loop there is an integral of a loop momentum, but only over its plus and transverse components: $\int \dfrac{\mathrm{d}k^+ \, \mathrm{d}^{n-2}\boldsymbol{k}_\mathrm{T}}{(2\pi)^{n-1}}$.
6. For each line l there is a factor $\dfrac{1}{2k_l^+}$.
7. For each intermediate state α there is a factor

$$\frac{i}{P_\alpha^- - P_{\alpha\ \text{on-shell}}^- + i0}. \tag{7.16}$$

Here P_α^- is the total *external* minus momentum entering the graph to the left (earlier x^+) than the intermediate state α, while $P_{\alpha\ \text{on-shell}}^-$ is the value of the minus momentum of the particles contained in the state when they are on-shell. That is,

$$P_{\alpha\ \text{on-shell}}^- = \sum_{l\in\alpha} \frac{k_{l\mathrm{T}}^2 + m_l^2}{2k_l^+}. \tag{7.17}$$

These rules can be derived by normal time-dependent perturbation theory, with the change that light-front quantization is used and the evolution variable is x^+ instead of ordinary time (Kogut and Soper, 1970). What we will do here instead is to derive them from Feynman perturbation theory in the coordinate-space representation, with the integrals

over the positions of the vertices split up according to their ordering in x^+. This second method directly shows the equivalence with Feynman perturbation theory; it will also provide techniques for analyzing Feynman graphs in terms of particles propagating in space-time.

Derivation

See also Ligterink and Bakker (1995) for a derivation.

We start with the momentum-space representation for Feynman graphs and perform appropriate Fourier transforms to obtain the coordinate-space representation, but only as regards plus components of vertex positions. In all of the following, we will use x_j to represent the position of a vertex j in a graph.

First we Fourier-transform a free propagator to plus position, and decompose according to the ordering of its vertices:

$$\tilde{G} \equiv \int \frac{\mathrm{d}k^-}{2\pi} e^{ik^-(x_j^+ - x_k^+)} \frac{i}{2k^+ k^- - k_\mathrm{T}^2 - m^2 + i0}$$

$$= \theta(x_k^+ - x_j^+) \frac{\theta(k^+)}{2k^+} e^{ik_\mathrm{on-shell}^-(x_j^+ - x_k^-)} + \theta(x_j^+ - x_k^+) \frac{\theta(-k^+)}{-2k^+} e^{i(-k)_\mathrm{on-shell}^-(x_k^+ - x_j^-)}. \quad (7.18)$$

Here k is regarded as flowing from x_j to x_k, and the explicit minus signs in the second term serve to indicate that we always have physical (positive) plus momentum flowing from the earlier vertex to the later vertex. The above formula is readily derived by contour integration.

So we decompose the free momentum-space propagator as

$$G = \frac{\theta(k^+)}{2k^+} \frac{i}{k^- - (k_\mathrm{T}^2 - m^2)/(2k^+) + i0} + \frac{\theta(-k^+)}{-2k^+} \frac{i}{-k^- - (k_\mathrm{T}^2 - m^2)/(-2k^+) + i0},$$
$$(7.19)$$

with each term being associated with one of the two possible x^+ orderings of the ends of the line.

A common textbook derivation of Feynman rules starts from the coordinate representation (from Wick's theorem or a similar result from the functional integral), and then writes the result in terms of Fourier transforms into momentum space. Here we first partially reverse the derivation by writing the delta function for conservation of minus momentum at a vertex j as

$$2\pi\delta\left(p_j^- + \sum k_{l\,\mathrm{in}}^- - \sum k_{l\,\mathrm{out}}^-\right) = \int \mathrm{d}x_j^+ \, e^{ix_j^+(-p_j^- - \sum k_{l\,\mathrm{in}}^- + \sum k_{l\,\mathrm{out}}^-)}, \quad (7.20)$$

where p_j^- is the external momentum entering at the vertex, the $k_{l\,\mathrm{in}}^-$ are the momenta on lines coming to the vertex from earlier vertices, and $k_{l\,\mathrm{out}}^-$ are the momenta on lines leaving the vertex on lines to later vertices. In this formulation we have an integral over the minus momentum of each and every line, with explicit delta functions at the vertices.

We next obtain the contribution from a particular ordering of the x_j^+. We choose the vertex labels to correspond to the ordering $x_1^+ < x_2^+ < x_3^+ \ldots$, and we implement this by
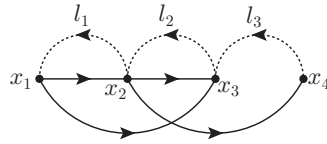
Fig. 7.4. Momentum-space representation of an x^+ ordering of a Feynman graph. See the text for explanation.

multiplying the original Feynman graph by theta functions: $\prod \theta(x_{j+1}^+ - x_j^+)$. Then we write a momentum-space representation for the theta functions:

$$\theta(x_{j+1}^+ - x_j^+) = \int \frac{dl_j^-}{2\pi} e^{il_j^-(x_j^+ - x_{j+1}^+)} \frac{i}{l_j^- + i0}. \tag{7.21}$$

We represent this in Fig. 7.4, where the dotted lines represent minus momenta flowing from each vertex to the next, together with the factor $i/(l_j^- + i0)$ in the above equation. Next to each vertex is a label for its position.

The integral over the vertex positions now gives us back conservation of minus momentum at each vertex, but with the momenta on the dotted theta-function lines included. We treat the minus momenta on the regular (non-dotted) lines as the independent variables of integration, with the vertex delta functions determining the l_j^- variables. If a line of momentum k goes from vertex j to a later vertex j', then k^- gets routed back along all the dotted lines from j' to j.

Finally, we apply contour integration on each k^- integral, closing in the lower half plane on the poles of the regular propagators. This then sets k^- in each of the dotted-line factors between j and j' to be the on-shell value. Repeating this for every line then results in the dotted line joining two vertices having a contribution of the on-shell k^- in the corresponding intermediate state. The momentum-conservation delta functions also route the external momenta along the dotted lines. Thus the final result is to turn the dotted-line factors into exactly the energy denominators we announced in the rules for x^+-ordered perturbation theory.

This completes the derivation.

Fermion lines

The numerator factor for a free fermion propagator G_f has k^- dependence, and this entails an extension to the decomposition (7.19) that we wrote for a scalar field propagator. We write the k^- dependence of the numerator as $i\gamma^+ k^- = i\gamma^+ k_{\text{on-shell}}^- + i\gamma^+(k^- - k_{\text{on-shell}}^-)$, where the first term works just as in the scalar propagator, but the second term cancels the on-shell pole, to give

$$G_f = \frac{\theta(k^+)}{2k^+} \frac{i(\slashed{k}_{\text{on-shell}} + m)}{k^- - (k_T^2 - m^2)/(2k^+) + i0} + \frac{\theta(-k^+)}{-2k^+} \frac{i(\slashed{k}_{\text{on-shell}} + m)}{-k^- - (k_T^2 - m^2)/(-2k^+) + i0}$$
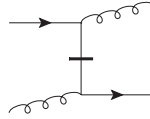
$$+ \frac{i\gamma^+}{2k^+}. \tag{7.22}$$

Fig. 7.5. Instantaneous interaction for fermion, denoted by the line with a bar across it. It has the value of $i\gamma^+/(2k^+)$ times the attached interaction vertices.

After the x^- integrals are performed, the last term Fourier-transforms to a delta function in x^+, giving an instantaneous interaction (Kogut and Soper, 1970) denoted diagrammatically by a line with a bar across it, as in Fig. 7.5. Naturally there is no associated intermediate state.

Similar issues arise with momentum-dependent vertices, as for the 3-gluon vertex in QCD and with couplings of gauge bosons to scalar fields.

7.2.4 Interpretation for pdf; time scales

Originally, the methods of x^+-ordered perturbation theory and its predecessor, the infinite-momentum technique, were applied to scattering processes at high energy. But as factorization theorems became systematized, the applications of x^+-ordered perturbation theory shifted more to treating the properties of a collinear region; more specifically, they became of use in analyzing the state of a fast-moving particle, e.g., the target in DIS.

An example is the calculation of a parton density, e.g., from Fig. 6.13. The two vertices defining the parton density are at equal x^+, and thus there is no intermediate state between them. In x^+-ordered perturbation theory the target splits into two particles. There is an intermediate state of the partons k and $P - k$ which propagates until one of the partons gets to the parton-density vertex. In the application of a pdf to DIS, this corresponds to where the virtual photon knocks out the parton, over a short time scale. Then the amplitude is squared to make a probability density. In the space-time picture of DIS, Fig. 6.3, the outgoing struck quark goes almost exactly in the x^- direction.

In the paradigmatic parton-model region, the incoming quark has transverse momentum of order a normal hadronic mass M. Then the denominator for the intermediate state in light-front perturbation theory is of order M^2/P^+, i.e., of order M^2x/Q in the Breit frame. We expect the typical lifetime of the state to be the inverse of this. This gives a typical intrinsic hadronic time scale $1/M$ times a time-dilation factor P^+/M. Thus x^+-ordered perturbation theory nicely and quantitatively implements the parton-model intuition. We can summarize the parton-model approximation as neglecting the duration of the hard collision compared with this long time scale P^+/M^2.

DIS exhibits the situation that in the interesting cases one always has at least two different directions of motion for the high-energy particles. While x^+-ordered perturbation theory is very natural for discussing the target state and its evolution, including that of the target remnant, a corresponding discussion of the outgoing struck quark is more naturally made with ordering with respect to the other light-front variable x^-. Naturally in more

complicated situations one has even more relevant directions for collinear sets of particles, and a correspondingly appropriate light-front variable for each set. Observe that discussion of the struck quark jet in DIS involves lines with plus momentum of order M^2/Q at large Q. Thus in the version of light-front perturbation theory appropriate to the *target*, the lines of the outgoing struck quark have close to zero plus momentum, i.e., they are close to the zero modes.

A unified description of the whole process is best made using ordinary Feynman perturbation theory, with light-front methods being applied separately to each collinear group (e.g., the target, or the outgoing struck quark together with its associated jet).

7.2.5 Frame dependence of ordering of x^+ and x^- in DIS

Consider the struck quark in DIS before it collides with the virtual photon in the parton-model region of low transverse momentum. In a Feynman graph its longitudinal momentum components have opposite signs: $k^+ > 0$, $k^- < 0$. This has the following interesting consequence.

In x^+-ordered perturbation theory, the parton travels forward from its last interaction inside the target, precisely because $k^+ > 0$. The value of k^- was integrated over to obtain this form of perturbation theory. Viewed in the Breit frame, this shows that the last interaction in the target happens earlier than the hard collision with the virtual photon.

Suppose instead we used x^--ordered perturbation theory. This would appropriate for discussing physics in the target rest frame, in which case the virtual photon is moving with large momentum in the *negative z* direction. The longitudinal variable parameterizing the parton state is now k^-. Since this is negative, the propagation is from the photon vertex to an interaction with the target. Thus the ordering of the events is reversed. This is illustrated in Fig. 7.6. We have thus found that the time-ordering of the ends of the line of momentum k gets reversed in different frames. This requires the separation of the ends to be space-like, and is specifically associated with the opposite signs of k^+ and k^-, and thus with the fact that the momentum of the line is space-like.

7.3 Light-front wave functions

7.3.1 Definitions

The treatment in this section is based on Brodsky and Lepage (1989) and Brodsky, Pauli, and Pinsky (1998), but the normalizations of the states and wave functions are adjusted to be Lorentz invariant.

In any quantum field theory, the states of the theory can be obtained by applying products of fields to the true vacuum and then taking linear combinations. A convenient basis with a Fock-space structure is made by using the creation operators obtained in light-front quantization.

Let us define basis states by applying bare creation operators to the true vacuum. We label the states by the particle type, their plus and transverse momenta, and helicities. For
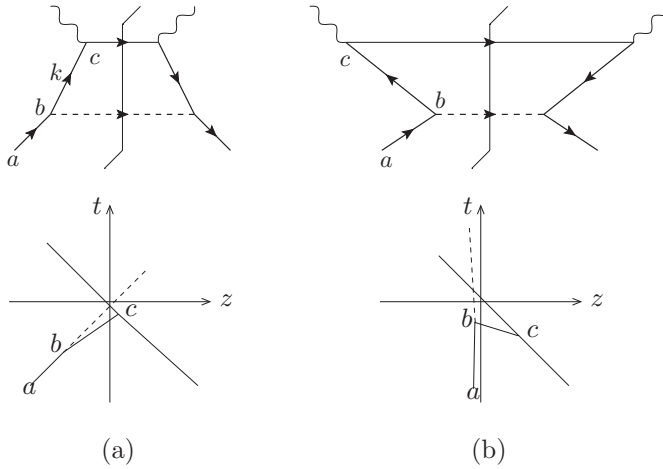
Fig. 7.6. x^+ and x^- ordering and DIS viewed in (a) the Breit frame, and (b) the target rest frame. The top line shows Feynman graphs organized for x^+- and x^--ordered perturbation theory, and the bottom line shows the positions of the vertices in space-time.

example, in the Yukawa theory treated in the previous chapter, the list of basis states would start as

$$
\begin{aligned}
&|0\rangle\,, \\
&|f:k,\alpha\rangle && = b^\dagger_{k,\alpha}|0\rangle\,, \\
&|s:k\rangle && = a^\dagger_k|0\rangle\,, \\
&|f\bar{f}:k_1,\alpha_1;k_2,\alpha_2\rangle = b^\dagger_{k_1,\alpha_1}d^\dagger_{k_2,\alpha_2}|0\rangle\,, \\
&|fs:k_1,\alpha_1;k_2\rangle && = b^\dagger_{k_1,\alpha_1}a^\dagger_{k_2}|0\rangle\,, \\
&\quad\ldots
\end{aligned}
\tag{7.23}
$$

Here f and s denote the fermion and the scalar particles, and α is for fermion helicity. The momentum label for each particle is of the form $k_j = (k_j^+, \boldsymbol{k}_{jT})$. Naturally, this generalizes to any theory, simply by the use of suitable particle labels. In a theory with color confinement, like QCD, it is necessary to restrict to color singlet states. (At this point we gloss over complications that happen in real QCD.)

We use bare creation operators, i.e., those obtained from the bare fields, so that they obey the standard (anti)commutation relations (6.65), and the states have standard orthonormality conditions, e.g.,

$$
\langle f:k',\alpha'|f:k,\alpha\rangle = (2\pi)^{n-1}2k^+\delta_{\alpha\alpha'}\delta(k'^+ - k^+)\delta^{(n-2)}(\boldsymbol{k}'_T - \boldsymbol{k}_T). \tag{7.24}
$$

A general single-particle state $|h:P\rangle$ of momentum P, with $\boldsymbol{P}_T = 0$, is expanded as

$$
|h:P\rangle = \sum_{F,\{\alpha_j\}}\int d[\{x,k_T\}]\,\big|F:\{x_jP^+, \boldsymbol{k}_{jT},\alpha_j\}\big\rangle\,\psi_{F/h}\big(\{x_j,\boldsymbol{k}_{jT},\alpha_j\}\big), \tag{7.25}
$$

where the sum is over the numbers of particles, and their types and helicities. The notation $\{\ldots\}$ denotes an array of single-particle quantities. The measure for the integral is

$$d[\{x_j, k_{j\,T}\}] \stackrel{\text{def}}{=} \frac{1}{\#(f)!\#(\bar{f})!\#(s)!} \prod_j \left(\frac{dx_j\, d^{n-2}k_{j\,T}}{2x_j(2\pi)^{n-1}} \right)$$

$$\times\, \delta\Big(1 - \sum_j x_j\Big) 2(2\pi)^{n-1}\delta^{(n-2)}\Big(\sum_j k_{j\,T}\Big), \quad (7.26)$$

with the factorials in the prefactor chosen to compensate the multiple counting of configurations of identical partons.

The decomposition (7.25) of a state $|h : P\rangle$ was defined to apply at $P_{\mathrm{T}} = 0$. It is left as an exercise (problem 7.4) to show that to obtain the state with non-zero P_{T} one makes the replacement

$$\psi_{F/h}(\{x_j, k_{j\,\mathrm{T}}, \alpha_j\}) \mapsto \psi_{F/h}(\{x_j, k_{j\,\mathrm{T}} - x_j P_{\mathrm{T}}, \alpha_j\}). \quad (7.27)$$

The coefficients $\psi_{F/h}(\{x_j, k_{j\,\mathrm{T}}, \alpha_j\})$ are called the light-front wave functions,[1] and they obey the normalization condition (to be proved in problem 7.4)

$$\sum_{F,\{\alpha_j\}} \int d[\{x, k_{\mathrm{T}}\}] \left| \psi_{F/h}(\{x_j, k_{j\,\mathrm{T}}, \alpha_j\}) \right|^2 = 1. \quad (7.28)$$

A projection onto basis states gives the wave functions

$$\langle F : \{x_j P^+, k_{j\,\mathrm{T}}, \alpha_j\} | h : P\rangle = \psi_{F/h}(\{x_j, k_{j\,\mathrm{T}}, \alpha_j\})$$

$$\times\, 2(2\pi)^{n-1}\delta\Big(1 - \sum_j x_j\Big)\delta^{(n-2)}\Big(\sum_j k_{j\,\mathrm{T}}\Big), \quad (7.29)$$

where we now assume $P_{\mathrm{T}} = 0$ again.

7.3.2 Uses

Light-front wave functions are directly used in factorization theorems for exclusive scattering. The parton densities can be expressed in terms of light-front wave functions (problem 7.6).

7.4 Light-front quantization in gauge theories

We have seen the value of light-front quantization in gaining understanding and intuition for the parton model. So in this section we examine its application to QCD. At first sight, if we use the light-cone gauge $A^+ = 0$, all the same considerations as we used above seem to apply. Notably, the same results about the number density interpretation of parton densities

---

[1] In (7.25) the measure was normalized to match the covariant normalization (7.24) for partonic states. Thus the normalization of the wave functions differs from those in Brodsky, Pauli, and Pinsky (1998) and Heinzl (2001).

appear to apply. However, a number of complications are caused by the use of light-cone gauge, symptomized by important divergences, as we will see strongly in later chapters.

Nevertheless, it is useful to make a start by ignoring the complications and divergences. Such an approach has been enormously influential. Among other things one gains candidate definitions of parton densities, of light-front wave functions, and of related quantities, not to mention substantial intuition and insight. The true results will be distortions of those presented here.

7.4.1 Light-cone gauge

For treating light-front quantization, on a null plane of constant x^+, it is convenient (Kogut and Soper, 1970; Srivastava and Brodsky, 2001) to use the gauge-fixing condition $A^+ = 0$: only transverse degrees of freedom propagate, and there are no Faddeev-Popov ghosts. This is the "light-cone gauge" or "light-like axial gauge".

The determining issue for using this gauge to treat parton physics is that the leading regions for DIS are then the same as in non-gauge theories. In contrast, in a general gauge, there are extra gluon lines attaching to the hard subgraph H in Fig. 5.7(c), and the leading part involves the plus component of gluon polarization, which vanishes in $A^+ = 0$ gauge.

We first examine this gauge (Bassetto *et al*., 1985; Leibbrandt, 1987) independently of the issues of light-front quantization and of parton physics. This can be done in a coordinate-independent and Lorentz covariant fashion by introducing a future-pointing light-like vector $n^\mu = \delta^\mu_-$, so that for any vector V we have $V^+ = n \cdot V$. The gauge condition is $n \cdot A = 0$, and a fractional longitudinal momentum is $\xi = k^+/P^+ = n \cdot k/n \cdot P$. Results for Green functions etc. are invariant under scaling of n by a positive real number.

There are no ghost fields in this gauge. The Feynman rules (Bassetto *et al*., 1985; Leibbrandt, 1987) are obtained from those in covariant gauges (Fig. 3.1) by making two changes: the Faddeev-Popov fields are removed, and the free gluon propagator is changed to

$$\frac{i\delta_{\alpha\beta}N_{\mu\nu}}{k^2 + i0},$$

(7.30)

where the numerator is

$$N_{\mu\nu} = -g_{\mu\nu} + \frac{k_\mu n_\nu + n_\mu k_\nu}{k \cdot n}.$$

(7.31)

The singularity at $k^+ = k \cdot n = 0$ causes problems. It is (Bassetto *et al*., 1985; Leibbrandt, 1987) to be defined as a principal value in loop integrals. In many cases this works and gives physical results equivalent to those in covariant gauge, despite some complications in renormalization (Bassetto, Dalbosco, and Soldati, 1987).

However, the gauge gives some non-trivial divergences in TMD parton densities, etc. See Ch. 13 for the non-trivial details and how this is related to physically observable effects.

$$\frac{}{} \;=\; \frac{in_\mu n_\nu}{(k \cdot n)^2}$$

Fig. 7.7. Instantaneous interaction for gluon, when x^+-ordered perturbation theory in light-cone gauge is used. This barred gluon connects two regular interaction vertices at equal values of x^+. The ends of the line are connected to any normal gluon-containing vertices.

7.4.2 Light-front perturbation theory for gauge theory

For the derivation of the x^+-ordered rules for perturbation theory, the k^- dependence of the numerator of the gluon propagator causes a complication. Just as with the fermion propagator, we will find we need an extra interaction, now with instantaneous gluon exchange. We derive it by extracting from the gluon numerator a term that contains the k^- dependence and that is proportional to the denominator, i.e., k^2. Thus we obtain a modified gluon numerator:

$$
\begin{aligned}
N_{\mu\nu}^{\text{lf pert.}} &= -g_{\mu\nu} + \frac{k_\mu n_\nu + n_\mu k_\nu}{k \cdot n} - \frac{k^2 n_\mu n_\nu}{(k \cdot n)^2} \\
&= -g_{\mu\nu} + \frac{k_\mu n_\nu + n_\mu k_\nu}{k \cdot n}\bigg|_{k^- \mapsto k_{\mathrm{T}}^2/2k^+}.
\end{aligned}
\tag{7.32}
$$

This does not affect the $k^2 = 0$ pole of the free gluon propagator, and is the appropriate form for making the transition to light-front perturbation theory (Srivastava and Brodsky, 2001). To keep the physical predictions of the theory the same, the extra term in the gluon propagator is compensated by an extra instantaneous interaction (Kogut and Soper, 1970). The new element in the Feynman rules, Fig. 7.7, corresponds to extra terms in the light-front Hamiltonian (Srivastava and Brodsky, 2001). See the quoted references for details. Note that in ordinary Feynman perturbation, the correct numerator is *not* (7.32), but is (7.31), with the ordinary interactions.

7.5 Parton densities in gauge theories

Initially we defined the parton density for a fermion as an expectation value of a certain bilocal operator, (6.31). This was motivated by the derivation of the parton model in a model field theory. We then saw that this parton density is an expectation value of a light-front number operator, (6.66), which is a natural implementation of the intuition embodied in the picture of scattering off constituents of the target.

For QCD, we could apply this same operator definition in $A^+ = 0$ gauge, because of the already mentioned simplification of the leading regions in this gauge. We simply modify the definition to include a sum over the three quark colors.

But we wish also to be able to use a general gauge. For this we need to find a gauge-invariant definition that agrees with (6.31) in $A^+ = 0$ gauge. As I now explain, this is

done (Collins and Soper, 1982b) by inserting between the $\bar{\psi}$ and ψ operators a suitable path-ordered exponential of the gluon field. Such an exponential is called a Wilson line.

7.5.1 Wilson lines

A general Wilson line[2] is defined as a path-ordered exponential of the integral of the gluon field (times generating matrix) along a line (or path) joining two points. If we parameterize a path C by a function $x^\mu(s)$ where s goes from 0 to 1, then the associated Wilson line is

$$W(C) \stackrel{\text{def}}{=} P\left\{\exp\left[-ig_0 \int_0^1 \mathrm{d}s \, \frac{\mathrm{d}x^\mu(s)}{\mathrm{d}s} A_{(0)\mu}^\alpha(x(s)) \, t_\alpha\right]\right\}, \tag{7.33}$$

which is more compactly written as

$$W(C) = P\left\{\exp\left[-ig_0 \int_C \mathrm{d}x^\mu \, A_{(0)\mu}^\alpha(x) \, t_\alpha\right]\right\}. \tag{7.34}$$

Here t_α are generating matrices of the gauge group, in the fundamental representation. The path-ordering symbol P means that when the exponential is expanded, the fields with higher values of s are to the left. The Wilson line is invariant if the path is reparameterized, but it does change if the location of the path is changed even with fixed endpoints.

Under a gauge transformation, the Wilson line transforms as

$$W(C) \mapsto e^{-ig_0 t^\alpha \omega_\alpha(x(1))} \, W(C) \, e^{ig_0 t^\alpha \omega_\alpha(x(0))}, \tag{7.35}$$

which involves only the transformations at the ends of the path. Note that it is the bare field and coupling that appear in the formula for $W(C)$, since the transformations giving invariance of the Lagrangian are those in (2.4) with bare gauge fields and couplings.

From the transformation of $W(C)$ it follows that if C is a path from v to w then the combination $\bar{\psi}(w)W(C)\psi(v)$ is gauge invariant.

A simple generalization is to replace t_α by the generating matrices in another representation. We use this for the gluon density, where the fields at the ends of the Wilson line are gluon field-strength tensors, and the Wilson line uses the adjoint representation.

7.5.2 Path dependence of Wilson line

In general $\bar{\psi}(w)W(C)\psi(v)$ depends not only on the endpoints v and w of the Wilson line, but also on the exact path used to join them.

However, for the case of the standard parton densities, a simplification occurs, because we use a light-like separation in the minus direction: $v = 0$ and $w = (0, w^-, \mathbf{0}_\mathrm{T})$, and it is appropriate to take the Wilson line along the x^- axis. In that case, we now show that the Wilson line depends only on the endpoints. This will enable us to obtain a useful simplification in the Feynman rules for the Wilson line.
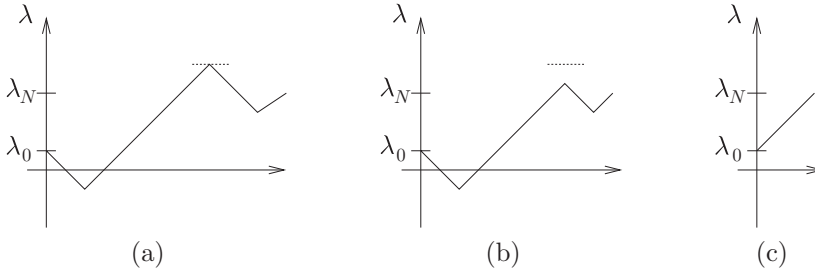
[2] Another commonly used name is a "gauge link".

Fig. 7.8. (a) Example of possible path for Wilson line along a single line, as in an ordinary pdf, but with possible backtracking. The vertical axis denotes the coordinate λ along the line. (b) The path altered by changing one of the extreme points. The original coordinate of the altered point is marked by the dotted line. (c) The path after removal of all backtracking. The corresponding Wilson-line factor is unchanged.

We now prove the following general result:

Let C be a path restricted to a line in a fixed direction n, so that points on the line can be written $w^\mu = \lambda n^\mu$. The path is a sequence of N segments joined by direct lines:

$$W(C) = \prod_{j=1}^{N} W(\lambda_j, \lambda_{j-1}), \tag{7.36}$$

where

$$W(\lambda_j, \lambda_{j-1}) \overset{\text{def}}{=} P\left\{ \exp\left[-i g_0 \int_{\lambda_{j-1}}^{\lambda_j} d\lambda\, n^\mu A^\alpha_{(0)\mu}(\lambda n)\, t_\alpha \right] \right\}. \tag{7.37}$$

Then $W(C)$ depends only on the endpoints:

$$W(C) = W(\lambda_N, \lambda_0). \tag{7.38}$$

We illustrate the proof in Fig. 7.8, where the path oscillates on its way from the start to the end, and does some backtracking.

The proof is made by differentiating $W(\lambda_{j+1}, \lambda_j)\, W(\lambda_j, \lambda_{j-1})$ with respect to λ_j, which gives zero. Thus the product is independent of λ_j, so that we can replace λ_j by λ_{j-1}, and we can remove the $W(\lambda_j, \lambda_{j-1})$ factor. Repeating this $N-2$ times gives the desired result.

Notice that this proof would not work if we tried to deform the path off the chosen line. For example, moving one of the break points $\lambda_j n$ off the line would shift positions of the gauge fields in the neighboring segments, and the differentiation would involve more than the endpoints of the factors $W(\lambda_j, \lambda_{j-1})$.

A particular case used in the parton densities, is to replace the direct line joining the endpoints by a trip to infinity and back:

$$W(\lambda_N, \lambda_0) = W(\lambda_N, +\infty) W(+\infty, \lambda_0) = [W(+\infty, \lambda_N)]^\dagger W(+\infty, \lambda_0). \tag{7.39}$$

7.5.3 Time ordering v. path ordering

Feynman rules apply to time-ordered Green functions, so conflicts can arise between the path ordering defining Wilson lines and the time ordering used for Green functions. In a

covariant gauge, the fields commute at space-like separation, so no conflict arises if we use Wilson lines in space-like directions. This will be the case for TMD densities (Ch. 13) and for the Sudakov form factor (Ch. 10).

For normal integrated parton densities, one uses light-like lines in the direction $n = (0, 1, \mathbf{0}_T)$. If any serious difficulty arises, we take the line as the limit from a space-like direction. We can also use the canonical commutation relations in light-front quantization, in which case the relevant field component $n \cdot A = A^+$ has zero commutator with the same field at different positions along the line.

Such issues can be problematic in a non-covariant gauge, where the commutators of elementary fields may be non-vanishing at space-like separation.

7.5.4 Gauge-invariant quark density in QCD

To define a quark density gauge-invariantly, we use (Collins and Soper, 1982b) a Wilson line exactly along the light-like line joining the quark and antiquark fields. Then the Wilson line uses only A^+ component of the gauge field, and is unity in $A^+ = 0$ gauge; thus the gauge-invariant definition reduces to the basic definition (6.31) in this gauge. The gauge-invariant definition is

$$f_{(0)\,j/h}(\xi) = \int \frac{\mathrm{d}w^-}{2\pi}\, e^{-i\xi P^+ w^-} \left\langle P \left| \overline{\psi}^{(0)}_j(0, w^-, \mathbf{0}_T) W(w^-, 0) \frac{\gamma^+}{2} \psi^{(0)}_j(0) \right| P \right\rangle_{\mathrm{c}}, \quad (7.40)$$

where

$$W(w^-, 0) = P\left\{ e^{-ig_0 \int_0^{w^-} \mathrm{d}y^-\, A^+_{(0)\alpha}(0, y^-, \mathbf{0}_T) t_\alpha} \right\}. \quad (7.41)$$

Here we have written the bare parton density, in which all the fields are bare fields, since this is the object to which the probability interpretation applies. In real QCD, in four space-time dimensions, there are UV divergences, so a complete definition requires us to apply renormalization to obtain our final and correct definition of the parton densities. The same applies in more elementary theories, as we will discuss later in Sec. 8.3.

The gluon operators in the Wilson line commute, so a time ordering can be applied to the definition without changing the value of the quark density, just as in Sec. 6.9.4. If we use a fixed ordering for the quark operators, with a final-state cut, then it is better to use a path that goes out to infinity on the left of the final-state cut and back to $(0, w^-, \mathbf{0}_T)$ on the right, as in (7.39). This does not change the value of the quark density, as shown in Sec. 7.5.2.

Antiquark densities are defined by exchanging the roles of the ψ and $\bar{\psi}$ fields, as in (6.33), or equivalently by going to negative ξ in the quark density and using (6.85). Gauge-invariant polarized quark densities are naturally defined by replacing γ^+ by the appropriate Dirac matrix, exactly unchanged from (6.35) and (6.36).

7.5.5 Gluon density

In light-cone gauge, A^+ is zero, while A^- is a field expressed in terms of other fields by a constraint equation. Therefore the independent components of the gluon field are its

transverse components A^j. Their free-field action is $\frac{1}{2}\sum_j g^{\mu\nu}\partial_\mu A^j \partial_\nu A^j$, the same as for two independent scalar fields. Thus the operator quantization conditions are the same as for scalar fields. In particular, the expression relating A^j to the light-front creation and annihilation operators is the same, as are the commutation relations. So the gluon density is the same as for a scalar field, (6.124), with a sum over colors and transverse indices:

$$f_{(0)\,g}(\xi) = \sum_{j,\alpha} \int \xi P^+ \frac{\mathrm{d}w^-}{2\pi} e^{-i\xi P^+ w^-} \langle P|A^j_{(0)\,\alpha}(0, w^-, \mathbf{0}_\mathrm{T}) A^j_{(0)\,\alpha}(0)|P\rangle_{\mathrm{lcg}}. \qquad (7.42)$$

See below for the polarized densities

To convert this to a gauge-invariant expression that has the same value in light-cone gauge, it is not enough just to insert a Wilson-line factor, because of the derivative term in the gauge transformation of the gluon field. Instead we observe that the bare field-strength tensor $G^{\mu\nu}_{(0)}$ transforms without a derivative, so that a gauge-invariant operator can be constructed by joining two field-strength tensors by a Wilson line. Naturally, the representation matrices in the Wilson line must be those for the adjoint representation. Next we observe that in light-cone gauge $G^{+j}_{(0)} = \partial^+ A^j_{(0)}$. In momentum space, this is $A^j_{(0)}$ times a factor of a plus component of momentum (up to a phase). Thus the gauge-invariant form of the bare gluon density is (Collins and Soper, 1982b)

$$f_{(0)\,g}(\xi) = \sum_{j,\alpha} \int \frac{\mathrm{d}w^-}{2\pi \xi P^+} e^{-i\xi P^+ w^-} \langle P|G^{+j}_{(0)\,\alpha}(0, w^-, \mathbf{0}_\mathrm{T}) W_A(w^-, 0)_{\alpha\beta} G^{+j}_{(0)\,\beta}(0)|P\rangle_\mathrm{c},$$

$$\qquad (7.43)$$

where the subscript A on W_A denotes that the Wilson line is in the adjoint representation.

Just as with a quark, the gluon has a polarization state described by a 2×2 density matrix. But because the gluon has spin 1 instead of spin $\frac{1}{2}$, the decomposition in terms of a Bloch vector is not appropriate, because of the different transformation properties under rotations. Proofs of the many unproved statements in the following discussion are left as an exercise (problem 7.10).

A convenient method starts by modifying (7.42) and (7.43) to provide the gluon density matrix $\rho_{g,j'j}$:

$$\rho_{g,j'j}(\xi, S) f_{(0)\,g}(\xi) = \sum_\alpha \xi P^+ \int \frac{\mathrm{d}w^-}{2\pi} e^{-i\xi P^+ w^-}$$

$$\times \langle P, S|G^{+j}_{(0)\,\alpha}(0, w^-, \mathbf{0}_\mathrm{T}) W_A(w^-, 0)_{\alpha\beta} G^{+j'}_{(0)\,\beta}(0)|P, S\rangle_\mathrm{c}. \qquad (7.44)$$

Here we have simply removed the sum over the transverse spin index of the gluon field and allowed the two fields to have independent indices. Naturally we now allow a polarization specified by S for the target state. Notice the reversal of the order of the indices j and j' between the left- and right-hand sides of the equation. The factor $f_{(0)\,g}$ on the left-hand side ensures that ρ has the unit trace appropriate to a density matrix. The density matrix is a function of the longitudinal momentum fraction of the gluon and of the spin state of the target. But the gluon density $f_{(0)\,g}$ is independent of the spin state of the target,

because it is the expectation value of an azimuthally symmetric operator, just like a quark density.

We next note that a gluon with a polarization vector $\boldsymbol{\epsilon}$ has a density matrix $\epsilon_{j'}^*\epsilon_j$, and in $A^+ = 0$ gauge, $\boldsymbol{\epsilon}$ is a 2-component transverse vector. Important pure states can be made with linear polarization, where both components are relatively real, and with circular polarization. A convenient decomposition of a general density matrix is in terms of a helicity α and a linear polarization $\boldsymbol{L}$:

$$\rho = \frac{1}{2}\begin{pmatrix} 1 + L_x^2 - L_y^2 & 2L_xL_y - i\alpha \\ 2L_xL_y + i\alpha & 1 - L_x^2 + L_y^2 \end{pmatrix}$$

$$= \frac{1}{2}\begin{pmatrix} 1 + |\boldsymbol{L}|^2\cos 2\phi & |\boldsymbol{L}|^2\sin 2\phi - i\alpha \\ |\boldsymbol{L}|^2\sin 2\phi + i\alpha & 1 - |\boldsymbol{L}|^2\cos 2\phi \end{pmatrix}, \tag{7.45}$$

where ϕ is the azimuthal angle of the linear polarization relative to the x axis, and there is a positivity restriction $|\boldsymbol{L}|^4 + \alpha^2 \leq 1$. The helicity terms give the imaginary part of the off-diagonal elements of ρ, and their sign arises from the polarization vectors $(\epsilon_x, \epsilon_y) \propto (1, i)/\sqrt{2}$ for helicity $+1$ and $(\epsilon_x, \epsilon_y) \propto (-1, i)/\sqrt{2}$ for helicity -1.

We can project the helicity part of ρ by using the matrix[3]

$$P_{11}^{\text{hel}} = P_{11}^{\text{hel}} = 0, \qquad P_{12}^{\text{hel}} = -i, \qquad P_{21}^{\text{hel}} = i, \tag{7.46}$$

to give

$$\alpha_g f_{(0)g}(\xi) = \sum_{j,j'=1}^{2} P_{jj'}^{\text{hel}} \int \frac{\mathrm{d}w^-}{2\pi\xi P^+} e^{-i\xi P^+ w^-}$$

$$\times \langle P, S | G_{(0)}^{+j}(0, w^-, \mathbf{0}_{\mathrm{T}}) W_A(w^-, 0) G_{(0)}^{+j'}(0) | P, S \rangle. \tag{7.47}$$

We can use parity invariance (actually parity and a $180°$ rotation in the (x, y) plane) to relate the parton densities in target states of opposite helicity. As with a quark, it follows that in a spin-$\frac{1}{2}$ target, like a proton, the gluon helicity is proportional to the target helicity, so that we can define the bare gluon helicity density $\Delta f_{(0)g}$ by

$$\alpha_g f_{(0)g}(\xi) = \alpha_{\text{target}} \Delta f_{(0)g}(\xi). \tag{7.48}$$

Then in a target state of maximal helicity, $\Delta f_{(0)g}$ has the interpretation of a helicity asymmetry: the number density of gluons polarized parallel to the target minus the number polarized antiparallel.

The linear polarization of a gluon can also be defined, but there is no standard definition of a corresponding parton density. It would have little practical use, because the linear polarization of a gluon is zero in the most important case of a spin-$\frac{1}{2}$ hadron, as follows from conservation of angular momentum about the z axis (Artru and Mekhfi, 1990). (Linear polarization is measured by an operator that flips helicity by two units. Since no helicity

---

[3] Note that the formula for this matrix in Brock *et al.* (1995) is incorrect.

Overall factors (case of unpolarized distribution):

$\gamma^+/2$ $\qquad\qquad\qquad\qquad\qquad$ $\delta_{jj'}/(\xi P^+)$

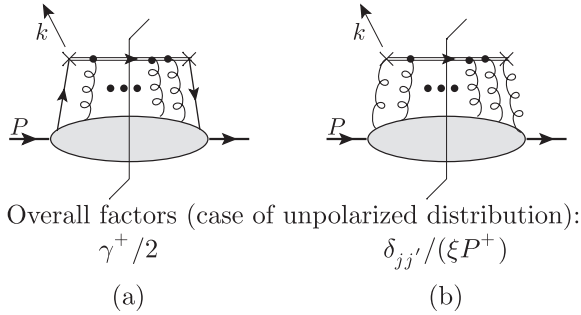(a) $\qquad\qquad\qquad\qquad\qquad\qquad$ (b)

Fig. 7.9. Feynman-graph notation for gauge-invariant (a) quark density, (b) gluon density. The double lines are for the Wilson lines, whose rules are in Figs. 7.10, 7.11, and 7.12. The short line at the top merely represents the flow of external momentum at the parton density vertex. The overall factors in the case of a quark are the same as in Fig. 6.7.

is absorbed by the azimuthally symmetric space-time part of the definition of the parton densities, the helicity flip in the operator equals the helicity flip in the density matrix for the hadron.)

In the occasionally used case of a spin-0 target (pion), the gluon is unpolarized, as follows by combining the above two arguments.

7.6 Feynman rules for gauge-invariant parton densities

To represent gauge-invariant parton densities in Feynman graphs, we notate the Wilson line by a double line joining the fields at the ends of the Wilson line, as in Fig. 7.9. Any number of gluons (zero or more) connect the Wilson line to the rest of the graph. An overall trace with a Dirac matrix in a quark density is independent of the presence of the Wilson line. To derive Feynman rules for the Wilson lines we expand the exponential of the field in powers of its argument. Each term gives a target matrix element of several gluon fields (and the fields at the ends of the Wilson line), integrated over certain positions. The factors of $-ig_0 A^+_{(0)\alpha} t_\alpha = -ig_0 n \cdot A_{(0)\alpha} t_\alpha$ result in the rules for vertices on the Wilson lines shown in Fig. 7.10. The rules are first written for bare fields. If we calculate with renormalized fields, the factor $Z_3^{1/2}$ in the relation between bare and renormalized gluon fields requires that we associate a factor $Z_3^{1/2}$ with each of the gluon fields in the rules for the parton density and the Wilson line, as shown in Fig. 7.10. The generating matrices t_α are those for the color representation of the quark or gluon whose density is being used, and these are multiplied along the Wilson line.

Next we write the Wilson line in the form of exponentials going to infinity, (7.39), we expand each exponential in a power series in its argument, and write the necessary coordinate-space Green function in terms of momentum-space Green function. The order g_0^n term has an integral over n coordinates. We express each integral as an integral over ordered variables, which cancels the factor $1/n!$ in the series expansion, and then we have
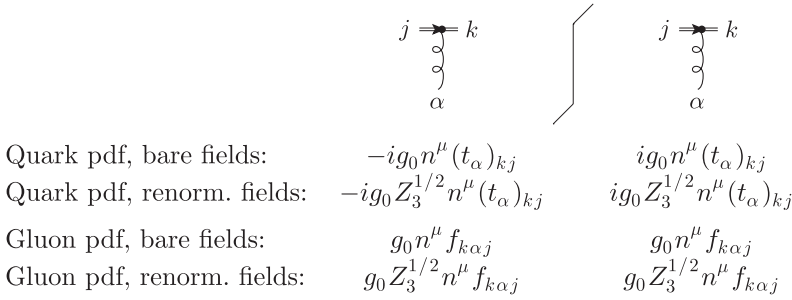
Quark pdf, bare fields:	$-ig_0 n^\mu (t_\alpha)_{kj}$	$ig_0 n^\mu (t_\alpha)_{kj}$
Quark pdf, renorm. fields:	$-ig_0 Z_3^{1/2} n^\mu (t_\alpha)_{kj}$	$ig_0 Z_3^{1/2} n^\mu (t_\alpha)_{kj}$
Gluon pdf, bare fields:	$g_0 n^\mu f_{k\alpha j}$	$g_0 n^\mu f_{k\alpha j}$
Gluon pdf, renorm. fields:	$g_0 Z_3^{1/2} n^\mu f_{k\alpha j}$	$g_0 Z_3^{1/2} n^\mu f_{k\alpha j}$

Fig. 7.10. Feynman rules for vertex on Wilson lines in parton densities. Here, $n^\mu = \delta_-^\mu = (0, 1, \mathbf{0}_{\mathrm{T}})$. In the Wilson line for a gluon pdf, the generating matrix for the adjoint representation was used: $(T_\alpha)_{kj} = i f_{k\alpha j}$. The sign of the vertex is reversed compared with Collins and Soper (1982b), and corresponds to the sign of the coupling in our Lagrangian, whose Feynman rules are in Fig. 3.1.

an integral of the form

$$\prod_j \int \frac{\mathrm{d}^{4-2\epsilon} k_j}{(2\pi)^{4-2\epsilon}} G(k_1, \mu_1, \alpha_1; \ldots) \prod_j (-ig_0 t_{\alpha_j} n^{\mu_j}) \int_0^\infty \mathrm{d}y_1^- \int_{y_1^-}^\infty \mathrm{d}y_2^- \ldots \int_{y_{n-1}^-}^\infty \mathrm{d}y_n^- \prod_j e^{ik_j^+ y_j^-}, \tag{7.49}$$

where G represents the rest of the graph, i.e., a shaded bubble in Fig. 7.9, including the lines connecting it to the Wilson line. This particular formula applies on the left of the final-state cut, with the gluon momenta k_j directed *down*, into the bubble. Applying the standard result

$$\int_z^\infty \mathrm{d}y \, e^{iky} = \frac{i}{k+i0} e^{ikz}, \tag{7.50}$$

gives a value for each double line segment shown in the left part of Fig. 7.11. Thus for the Wilson line on the left of the cut

$$= (-ig_0 t_{\alpha_n} n^{\mu_n}) \frac{i}{k_n^+ + i0} (-ig_0 t_{\alpha_{n-1}} n^{\mu_{n-1}}) \frac{i}{k_n^+ + k_{n-1}^+ + i0}$$

$$\times \cdots \times (-ig_0 t_{\alpha_1} n^{\mu_1}) \frac{i}{k_n^+ + \cdots + k_1^+ + i0}. \tag{7.51}$$

So the double lines in Fig. 7.9 behave like normal lines in a Feynman graph, with circulating loop momenta etc., but with a propagator that is the Fourier transform of a theta function. Of course the whole Wilson-line structure occurs once in the parton density and therefore once in the Feynman graph. There is naturally a hermitian conjugation of the above rules in the part of graphs to the *right* of the final-state cut, as usual, and as indicated in the figures.

In the definition of a parton density there is an integral over the external k^- and $\mathbf{k}_{\mathrm{T}}$. Since the Wilson-line propagator is independent of these momentum components, the integral
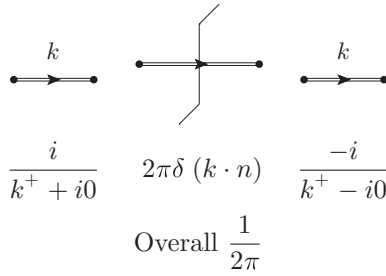
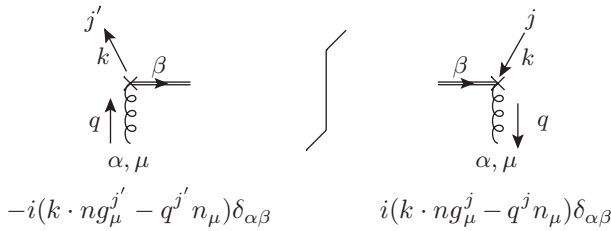Fig. 7.11. Feynman rules for the line part of a Wilson line.

Fig. 7.12. Feynman rules for attachment of gluon at end of Wilson line in gluon density. The indices α and β are for color, μ is the Lorentz index of the gluon, and j and j' are as in (7.44).

over them can be conveniently notated by routing them along the Wilson line and across the final-state cut. We give the cut line the natural delta function $2\pi\delta(k^+)$ for a cut propagator, and then we simply have to extract plus momentum ξP^+ at the end of the Wilson line. We also have to cancel the 2π in the cut-line propagator, as indicated in Fig. 7.11. This in fact results from the explicit factor $1/(2\pi)$ in the definitions of the parton density, e.g., (7.40).

The above completes the definition of the quark density. For the gluon density, we also need the vertex with $G_{(0)\,\alpha}^{+j} = \partial^+ A_{(0)\,\alpha}^j - \partial^j A_{(0)\,\alpha}^+ - g_0 f_{\alpha\beta\gamma} A_{(0)\,\beta}^+ A_{(0)\,\gamma}^j$, shown in Fig. 7.12. The derivatives give factors of $-iq^+$ and $-iq^j$, with q being the momentum of the gluon line. We apparently also need a two-gluon coupling at the end of the Wilson line. But we remove it (Collins and Soper, 1982b) by using the identity

$$\partial^+ \left(A_{(0)\,\alpha}^j(w^-) W_A(w^-) \right) = \left(\partial^+ A_{(0)\,\alpha}^j(w^-) - g_0 f_{\alpha\beta\gamma} A_{(0)\,\beta}^+ A_{(0)\,\gamma}^j \right) W_A(w^-), \qquad (7.52)$$

which accounts for the appearance of $k \cdot n$ rather than $q \cdot n$ in Fig. 7.12.

The application of the above rules will be illustrated by calculational examples in Sec. 9.4.

7.7 Interpretation of Wilson lines within parton model

Our first definition of a quark density was without a Wilson line and it arose from examining a theory in which DIS structure functions are dominated by the handbag diagram,
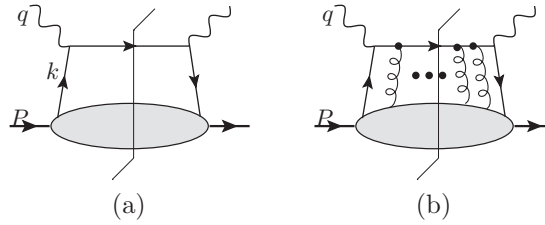
Fig. 7.13. Handbag graph: (a) standard, (b) with extra gluon exchanges.

Fig. 7.13(a), with the exchanged quark collinear to the target. Making suitable approximations converted the top of the diagram to a coefficient times the vertex for the quark density. In a gauge theory, this procedure gives the term in the quark density that has no gluons attached to the Wilson line.

We now show how there arise the terms with gluons attached to the Wilson line, as in Fig. 7.9. In a gauge theory in Feynman gauge, we have leading regions in which extra gluons couple the collinear subgraph to the hard subgraph. So we examine the generalized handbag diagrams shown in Fig. 7.13(b), where arbitrarily many gluons are exchanged between the top rung and the lower bubble. This provides a gauge-invariant extension of the parton model. In real QCD, we will also need more complicated hard-scattering graphs.

The extra gluons are to be collinear to the target, just like the exchanged quark, and we now show that to the leading power of Q, each of these graphs gives a corresponding term in the quark density, Fig. 7.9(a), times the same coefficient as with the handbag diagram. That this result is expected, since in $A^+ = 0$ gauge, the gluon-exchange graphs in the structure function are suppressed, and the gluon couplings to the Wilson line are zero.

To formalize the result, let $F_{[N]}(x, Q)$ be the contribution to a structure function from graphs of the form of Fig. 7.13(b) with N gluons attached to the upper line. Similarly, let $f_{[N],j}(x)$ be contribution to the parton density for a quark of flavor j with N gluons attached to the Wilson line. Then the result to be proved is that

$$F_{[N]}(x, Q) = \sum_j C_j f_{[N],j}(x) + \text{p.s.c.} \tag{7.53}$$

The important property is that the coefficient C_j is the same no matter how many gluons are exchanged. By "p.s.c." are denoted power-suppressed corrections, i.e., corrections suppressed by a power of Q. When we sum over N, on the left-hand side we get the full structure function $\sum_{N=0}^{\infty} F_{[N]} = F$. The sum of the right-hand side gives the full gauge-invariant parton density: $\sum_{N=0}^{\infty} f_{[N],j} = f_j$, multiplied by C_j. Thus we recover the standard parton-model formulae for the structure functions (6.25). The independence of the coefficient from N implies that it is correctly calculated from the case $N = 0$, and that it is the same as in the simple parton model, e.g., $C_j = e_j^2 x$ for the F_2 structure function in electromagnetic DIS.
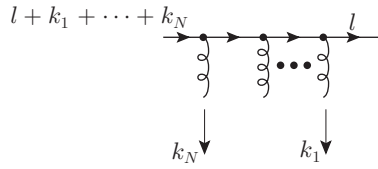
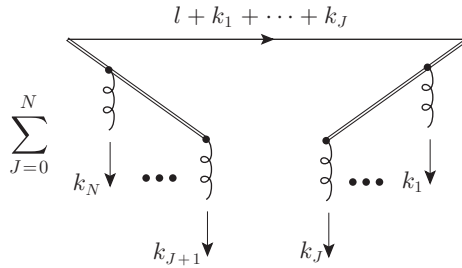Fig. 7.14. Attachment of collinear gluons to hard quark.

Fig. 7.15. Result of applying collinear approximation to Fig. 7.14. The double lines represent Feynman rules for a Wilson line on the left and for a conjugate Wilson line on the right.

The proof of (7.53) uses a result of Collins and Soper (1981) illustrated in Figs. 7.14 and 7.15. We write an upper quark line, Fig. 7.14, for the generalized handbag graph, as

$$U_N = \prod_j \left(-i g_0 t_{\alpha_j}\right) \frac{i}{\not{l} - m + i0} \gamma^{\mu_1} \frac{i}{\not{l} + \not{k}_1 - m + i0} \cdots \gamma^{\mu_n} \frac{i}{\not{l} + \not{k}_1 + \ldots \not{k}_N - m + i0}. \tag{7.54}$$

Since all the gluons are target-collinear, we can replace each gluon momentum by its plus component: $k_j \mapsto \hat{k}_j \stackrel{\text{def}}{=} (k_j^+, 0, \mathbf{0}_{\text{T}})$, and we can restrict the Dirac matrices at the vertices to their minus components: $\gamma^{\mu_j} \mapsto n^{\mu_j} \gamma^-$, where $n = (0, 1, \mathbf{0}_{\text{T}})$, as defined earlier. The resulting approximation to the quark line is

$$\hat{U}_N = \prod_j \left(-i g_0 n^{\mu_j} t_{\alpha_j}\right) W_N, \tag{7.55}$$

where

$$W_N = \frac{i}{\not{l} - m + i0} \gamma^- \frac{i}{\not{l} + \hat{\not{k}}_1 - m + i0} \gamma^- \cdots \gamma^- \frac{i}{\not{l} + \hat{\not{k}}_1 + \cdots + \hat{\not{k}}_N - m + i0}. \tag{7.56}$$

With a proof summarized below, this can be rewritten as

$$W_N = \sum_{J=0}^{N} R_J M_J L_{N,J}, \tag{7.57}$$

which we write as a diagram in Fig. 7.15, where the left-side factor is

$$L_{N,J} = \frac{i}{k_{J+1}^+ + i0} \cdots \frac{i}{k_{J+1}^+ + \cdots + k_N^+ + i0}, \qquad (7.58)$$

the middle factor is

$$M_J = \frac{i}{\rlap{/}{l} + \hat{k}_1 + \cdots + \hat{k}_J - m + i0}, \qquad (7.59)$$

and the right-side factor is

$$R_J = \frac{-i}{k_J^+ + i0} \cdots \frac{-i}{k_1^+ + \cdots + k_J^+ + i0}, \qquad (7.60)$$

Note that because of the standard conventions for lines for Dirac particles, the ordering of the objects is reversed between the equation and the diagram. "Right" and "left" refer to the sides of the diagram, not the formula.

The proof of (7.57) is by induction on N. The formula is trivially true for $N = 0$. Suppose that (7.57) is true for W_{N-1}. Then

$$W_N = W_{N-1}\gamma^- M_N$$

$$= \sum_{J=0}^{N-1} R_J M_J L_{N-1,J} \left(\frac{1}{M_N} - \frac{1}{M_J} \right) \frac{i}{k_{J+1}^+ + \cdots + k_N^+ + i0} M_N$$

$$= \sum_{J=0}^{N-1} R_J M_J L_{N,J} - \sum_{J=0}^{N-1} R_J L_{N,J} M_N. \qquad (7.61)$$

In the second line, we replaced γ^- by $(\hat{k}_{J+1} + \cdots + \hat{k}_N)/(k_{J+1}^+ + \cdots + k_N^+)$, and then wrote $\hat{k}_{J+1} + \cdots + \hat{k}_N$ as the difference of two inverse propagators. To complete the proof of (7.57), we use the result

$$\sum_{J=0}^{N} R_J L_{N,J} = 0 \qquad \text{if } N \geq 1, \qquad (7.62)$$

also proved by induction.

The double lines in Fig. 7.15 have the Feynman rules for a Wilson line on the left and a conjugate Wilson line on the right, with the Wilson lines going in the minus direction out to infinity.

We now apply (7.57) to the upper quark line on the left of the final-state cut in Fig. 7.13(b). Since the quark at the final-state end is on-shell, the only surviving term in Fig. 7.15 is where the Wilson-line factor is at the left, next to the current vertex. Similarly, applying (7.57) to the upper quark line on the right of the final-state cut gives a Wilson-line factor at the right of the line (again, next to the current vertex).

The result is to give a factor of the lowest-order hard scattering times a factor corresponding to the rules for the gauge-invariant quark density defined in (7.40), with the application of (7.39) to write the Wilson line as one that goes out to infinity and comes back. The $i0$
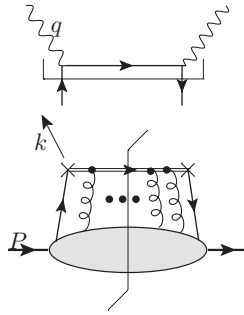
Fig. 7.16. Gauge-invariant form of the parton model.

prescription is chosen to be compatible with a deformation out of the Glauber region away from final-state poles. This is the appropriate direction, as we will see in Ch. 13.

We have now completed the derivation of the parton-model approximation in its gauge-invariant form, illustrated in Fig. 7.16. The coefficient function is the same as without the gluon exchanges.

Exercises

7.1 Verify that performing the $\boldsymbol{k}_{\mathrm{T}}$ integral in (7.13) does reproduce the result of applying the Feynman parameter method to (7.12).

7.2 Find in the literature or derive the full rules for x^+-ordered perturbation theory in a general renormalizable gauge theory, including a proper treatment of the 3-gauge field vertex and the coupling of gauge fields to scalar fields.

7.3 Verify that (7.28) follows from (7.25), the (anti)commutation relations (6.65), and the standard covariant normalization of a single particle state $|h : P\rangle$. Suggestion: investigate $\langle h : P'|h : P\rangle$.

7.4 (a) Find the general form of Lorentz transformations that preserve the plane $x^+ = 0$. Use one such transformation to transform the state $|h : P\rangle$ in (7.25) with $\boldsymbol{P}_{\mathrm{T}} = 0$ to a general value of P with non-zero $\boldsymbol{P}_{\mathrm{T}}$.

(b) The wave-function decomposition (7.25) of a state $|h : P\rangle$ was intended to apply at $\boldsymbol{P}_{\mathrm{T}} = 0$. Show that it also applies at non-zero $\boldsymbol{P}_{\mathrm{T}}$ if the replacement (7.27) is made.

(c) Obtain $\langle h, P'|h, P\rangle$, and deduce the normalization condition (7.28) from the Lorentz-invariant normalization (A.14) for single-particle states.

7.5 Express the lelt-hand side of (7.29) in terms of field operators in momentum space, integrated over k_j^-.

7.6 Derive an expression for the unintegrated parton densities $f_{j/h}(\xi, k_{\mathrm{T}})$ in terms of the light-front wave functions in (7.25). The result should be of the form of an

integral over $\left|\psi_{F/h}\bigl(\{x_j, \boldsymbol{k}_{j\,\mathrm{T}}, \alpha_j\}\bigr)\right|^2$, with the values of one of the x_j, $\boldsymbol{k}_{j\,\mathrm{T}}$ pairs set to ξ, $\boldsymbol{k}_{\mathrm{T}}$.

7.7 Obtain Feynman rules for computing light-front wave functions in perturbation theory; these will generalize the rules we constructed for parton densities in Sec. 6.10.

7.8 Apply them to the first non-trivial order in the Yukawa field theory we have used for examples. Verify the normalization condition (7.28). (Warning: Use dimensional regularization, so that the calculations can be done in the UV-regulated bare theory.)

7.9 In the parton model for CC processes with production of a heavy quark, in Sec. 7.1.3, we effectively assumed that the quark flavor and mass eigenstates coincided. In other words we assumed that the CKM matrix is unity. Correct the calculation to use a non-trivial CKM matrix.

7.10 Derive all the statements about polarized gluon densities in Sec. 7.5.5. *Check carefully the signs in the polarization vectors for gluons of definite light-front helicity*. You should be able to verify that there is a sign error in the formula for P^{hel} in Brock *et al.* (1995), and hence in the formula in that paper for Δf_g. [Thanks are due to Markus Diehl (private communication) for pointing out the error.]

7.11 As mentioned in Sec. 7.5.5, a linear polarization is possible for the gluon (although not in a spin-$\frac{1}{2}$ target). Work out the appropriate generalization of the work in this chapter to deal with this. An alternative formulation is in a helicity-density-matrix formalism, where linear polarization corresponds to a term with a gluon helicity flip of 2 units. If you get stuck, consult Artru and Mekhfi (1990).

7.12 Complete the derivations of (7.57) and (7.62).